

A Novel Method of Removing the Influence of Continuous Electromagnetic Wave Disturbances in OFDM Systems

Aleksandr Ovechkin, *Student Member, IEEE*, Tim Claeys *Member, IEEE*, Dries Vanoost *Member, IEEE*, Guy A. E. Vandenbosch *Fellow, IEEE*, and Davy Pissoort *Senior Member, IEEE*

Abstract—This paper describes a novel technique for removing the influence of a continuous wave (or narrowband) electromagnetic disturbance in orthogonal frequency division multiplexing (OFDM) systems with quadrature amplitude modulation (QAM) or phase-shift keying (PSK) modulation schemes. The technique relies on a mathematical derivation of how a continuous wave electromagnetic disturbance induces spectral leakage in the OFDM system. Using this derivation, an algorithm is obtained that aims to cancel the continuous wave electromagnetic disturbance by estimating its frequency, retrieving its amplitude and phase from the corrupted OFDM frame. Note that the algorithm does not require any prior information about the disturbance. The proposed algorithm is validated through thorough simulations, covering different modulations, noise variations and spectral leakage cases, and compared with standard OFDM performance without the algorithm. Through our experimentation it has been demonstrated that for a disturbance frequency not equal to one of the OFDM subcarriers, the algorithm can estimate the disturbance frequency with high precision, resulting in a gain of more than 80 dB when compared to the case without the algorithm. For a disturbance frequency equal to one of the OFDM subcarriers, a simple coding technique such as Hamming & interleaving enables the user to remove the disturbance.

Index Terms—Orthogonal frequency division multiplexing (OFDM), continuous wave noise, electromagnetic disturbance (EMD), narrowband interference (NBI), noise cancellation

I. INTRODUCTION

Wireless communication has become ubiquitous and is one of the most common forms in use today. It covers all aspects of modern life, from infotainment services (streaming platforms, social networks) to military and space implementations. Wireless connectivity is also being heavily incorporated into autonomous systems including automobiles. Within the automotive sector, there are six levels of automation [1]. The 6th level does not require any supervision or a human-in-the-loop that presents significant engineering challenges, including among other things, electromagnetic compatibility (EMC), reliability and safety. The IEEE 802.11bd and 5G NR protocols are seen as the most probable ones to be used

in autonomous vehicles [2]. The communication basis for these protocols is orthogonal frequency division multiplexing (OFDM) [3].

OFDM divides its bandwidth into multiple subcarriers orthogonal to each other, allowing to eliminate guard intervals between subcarriers (which are used in frequency division multiplexing) and increase the bandwidth efficiency. By introducing orthogonal subcarriers, an OFDM system can reduce the intersymbol interference (ISI) due to multipath fading to a bare minimum [3]. However, despite all its advantages, OFDM is not flawless and has drawbacks such as sensitivity to Doppler shift and frequency synchronization, high peak-to-average-power ratio (PAPR) and a decrease in efficiency due to the implementation of guard intervals [3].

The two new previously mentioned communication protocols (IEEE802.11bd and 5G NR) will be used in vehicle-to-everything (V2X) communication. Their main features are evaluated in [2]. However, the authors of [2] do not consider EMD in the shape of a narrowband continuous wave (CW) electromagnetic disturbance (EMD). In [4], the authors suggested a simulation and measurement strategy to evaluate the current protocols and possible improvements. This paper uses this strategy to evaluate such an improvement.

A CW EMD represents a signal that has a constant amplitude, phase, and frequency. This interference can be unintentional and coincide with the wireless communication frequency band, or it can be a so-called "jammer" [5], [6] that could intentionally generate it. That is why CW EMD is sometimes called a "constant jammer" [7].

The influence of CW EMDs on wireless communication systems is certainly not a new concern and has already been the focus of previous research. For example, in [8] the authors analyzed a long-term evolution (LTE) system intended for use in future vehicle applications. They investigated its susceptibility to different types of EMD, including CW EMD. They concluded that CW EMD has the most influence on LTE systems when the disturbance occurs in between two adjacent subcarriers.

In [9], the authors investigated the influence of CW EMD on OFDM systems in general. The authors conducted a number of simulations corrupting an OFDM signal with a CW EMD at different frequencies between two adjacent subcarriers. The results confirmed the findings achieved in [8] and showed that for an equal amount of power, a CW EMD degrades the performance of OFDM much more than, e.g. a broadband

The research leading to these results has received funding from the European Union's Horizon 2020 research and innovation programme under the Marie Skłodowska-Curie Grant Agreement No 812.788 (MSCA-ETN SAS). This publication reflects only the authors' view, exempting the European Union from any liability. Project website: <http://etn-sas.eu>

A. Ovechkin, T. Claeys, D. Vanoost and D. Pissoort are with ESAT-WaveCoRe, M-Group, KU Leuven Bruges Campus, 8000 Bruges, Belgium.

G. A. E. Vandenbosch is with ESAT-WaveCoRe, KU Leuven, 3000 Leuven, Belgium.

additive white Gaussian noise (AWGN). In [9], the authors showed that 5G NR did not consider that the impact, that CW EMD has, heavily depends on the disturbance's exact frequency position.

The current state-of-the-art CW EMD mitigation techniques can be divided into two groups:

- 1) Cancellation based on:
 - a) estimation [10], [11];
 - b) spectral leakage property [12];
 - c) soft/hard decision [13], [14].
- 2) Filtering [15], [16].

However, all the aforementioned techniques are based on several assumptions:

- 1) the methods described in [11] and [12] assume that the CW EMD frequency is known in advance;
- 2) in [10], the estimation of the CW noise frequency through interpolation [17] is based on prior information about the CW EMD power spectral density (PSD);
- 3) the techniques in [13] and [14] rely on the fact that the first decoded subcarriers of an OFDM frame should be the most reliable with the highest signal-to-interference-plus-noise (SINR) ratio;
- 4) in [15], the filter has to pass a learning phase achieved by sending 1000 signal-free training samples at the beginning of each OFDM packet.

Considering that the data rate (so and the symbol rate Bd) in modern OFDM systems is high, one may assume that the EMD within one OFDM frame remains constant (CW EMD). The algorithm proposed in this paper exploits this assumption and does not require any additional filters or prior information about the disturbance.

The remainder of this paper is organized as follows: Section II includes a mathematical explanation of the algorithm and its work principles, which is crucial for understanding the further sections. Section III proposes the simulation setup and clarifies the main parameters under which the algorithm was tested. Simulation results and an evaluation of the proposed CW EMD cancellation are also presented in Section III. Finally, Section IV draws concluding remarks. In what follows, the $*$ sign is used to indicate an estimation of a variable at the receiver's side (i.e. the estimation of E_m is defined as E_m^*).

II. DESCRIPTION OF THE ALGORITHM

A. OFDM frame transmission

For better comprehension of this section, a basic OFDM communication system is shown in Fig. 1. It represents the transmitter and the receiver of the communication system under consideration. Note that some blocks of this system were deliberately omitted to simplify the following explanation. Binary input data are modulated using a quadrature amplitude modulation (QAM) or phase-shift keying (PSK) modulator and represented as the complex number $S_k = I_k + jQ_k$, where k represents the subcarrier number. K symbols are then used as an input of the inverse discrete Fourier transform (IDFT) having a size of K samples in time as an output.

Each n^{th} sample after the IDFT block can be written as:

$$x_n = \frac{1}{K} \sum_{k=0}^{K-1} (I_k + jQ_k) e^{j2\pi kn/K} = a_n + jb_n, \quad (1)$$

where x_n is the current OFDM sample.

It is assumed that the system is fully synchronized in both the time and frequency domain. Cyclic prefixes or pilot symbols are not implemented since we consider perfect multipath fading equalization. The OFDM samples x_n are then mixed to the passband carrier frequency f_c , as shown in (2), and transmitted through the air using an antenna.

$$s_n = a_n \cos(2\pi f_c t) + b_n \sin(2\pi f_c t). \quad (2)$$

During the transmission, the CW EMD, defined in (3) as $n(t)$, is added to the time-domain OFDM signal $s_n(t)$, resulting in the received time-domain signal $z_n(t)$ as defined in (4):

$$n(t) = A_{CW} \cos(2\pi f_{CW} t + \theta_{CW}) \quad (3)$$

$$z_n(t) = s_n(t) + n(t). \quad (4)$$

In (3), A_{CW} denotes the noise amplitude, θ_{CW} and f_{CW} represent the phase and noise frequency, respectively. This frequency f_{CW} can be derived in terms of f_c . Let f_{diff} be the difference between f_c and f_{CW} , so that $f_{diff} = f_{CW} - f_c$. Then f_{diff} can be split into the sum of two parameters:

$$f_{diff} = (d + \alpha)H, \quad (5)$$

where H is the subcarrier spacing defined as $\frac{Bd}{K}$, in which Bd is the symbol rate or the baud rate. The symbol d is an integer number, such that $d \in [-K/2; K/2 - 2]$. Note that K should be even. The parameter α defines the position of the CW EMD between the two subcarriers d and $d + 1$ (see Fig.2a) and is within the range $[0 : 1[$. Note that when $\alpha = 0$, the CW EMD is located exactly on the subcarrier and only for the subcarrier (coherent sampling) with which f_{CW} coincides; an error value is added (shown in Fig. 2b). All the other α values result in spectral leakage (non-coherent sampling resulting in CW EMD power leakage) and add an error value to all subcarriers (shown in Fig. 2a). The algorithm presented in this paper exploits this phenomenon for OFDM communication and broadens the work presented in [18] and [19], where the spectral leakage phenomenon was exploited to analyze the signal measured in time-domain near-field scanning.

At the receiver, samples are converted back to the baseband frequency as:

$$r_n = z_n \cos(2\pi f_c t) + jz_n \sin(2\pi f_c t). \quad (6)$$

After filtering out the high frequency components (higher than f_c), the received baseband signal becomes:

$$\begin{aligned} r_n &= \frac{a_n}{2} + j\frac{b_n}{2} + \frac{A_{CW}}{2} \left(\cos(2\pi f_c t - 2\pi f_{CW} t - \theta_{CW}) \right. \\ &\quad \left. + j \sin(2\pi f_c t - 2\pi f_{CW} t - \theta_{CW}) \right) \\ &= \frac{a_n}{2} + j\frac{b_n}{2} + \frac{A_{CW}}{2} \left(\cos(2\pi f_{diff} t + \theta_{CW}) \right. \\ &\quad \left. - j \sin(2\pi f_{diff} t + \theta_{CW}) \right). \end{aligned} \quad (7)$$

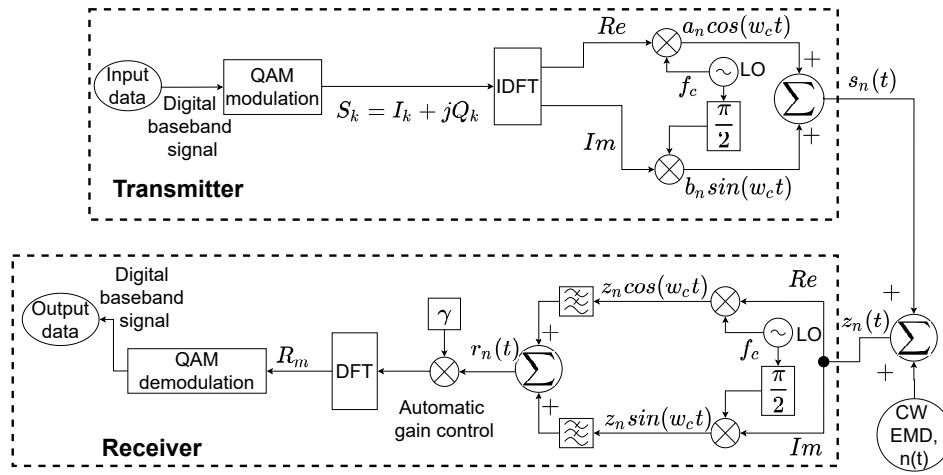


Fig. 1: OFDM communication system

The received K samples are then transformed back to the frequency domain using a discrete Fourier transform (DFT) with ideal automatic gain control to remove the division by two, as shown in (8):

$$R_m = \sum_{n=0}^{K-1} 2r_n e^{-j2\pi mn/K}, \quad (8)$$

where R_m is the received OFDM symbol, and m is the subcarrier.

B. Extracting the CW EMD from the OFDM frame

The received samples after the DFT block derived with (8) can be represented as the sum of two components: the symbol component S_m and the CW EMD component E_m as shown in (9):

$$R_m = S_m + E_m. \quad (9)$$

Depending on the CW EMD power, the symbols after QAM demodulation can either be erroneous or correct. If they are correct, then the QAM demodulation itself is not affected by the CW EMD component E_m and maps the received symbols back to original symbols S_m . However, at a certain power level, the CW EMD component introduces symbol flips, resulting in erroneous demodulation. In that case, the communication is impaired. Fig. 3 illustrates this, where the quadrature phase-shift keying (QPSK) modulated symbols were smeared with CW at 2 dB signal-to-interference ratio (SIR). The dashed black line subdivides Fig. 3 into four quadrants inside which there are four QPSK modulated symbols (blue circles), shown for reference. If a disturbed QPSK symbol (red circle) does not leave the reference signal's quadrant, then the demodulation results in correct symbols. If not, as it is in the bottom-right quadrant (there are two red symbols), then the demodulated symbol is erroneous. The CW EMD component E_m is shown as the vector \vec{E} with a solid line. All QPSK symbols are affected by CW EMD (look at $\vec{E}_{1,2,3,4}$), yet only one symbol, namely the first, leads to a symbol flip. Let us look at the disturbed symbol. The actual distances of the first reference (sent) and disturbed (received) QPSK symbols are shown with vectors \vec{S}_1 and \vec{R}_1 , respectively. The QPSK demodulator cannot identify the actual E_2 and S_2 values. Instead, it maps the received 1' symbol back to the QPSK symbol 4 in the bottom-right quadrant and will estimate the original vectors \vec{S}_1 and \vec{E}_1 as the new \vec{S}_1^* and \vec{E}_1^* vectors.

The CW EMD can be derived if one were to assume that the CW EMD component is small enough not to cause any

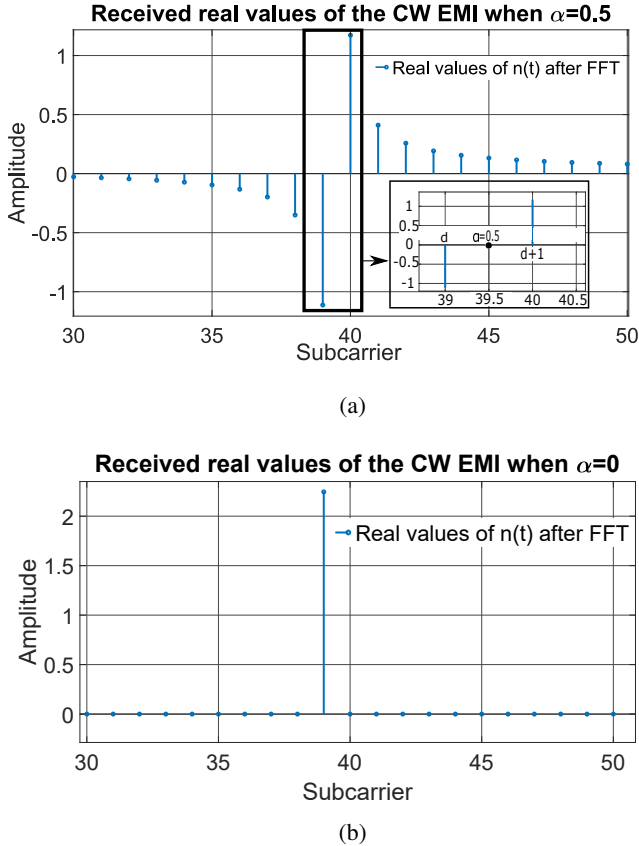


Fig. 2: Real values of CW EMD after DFT at the 39th subcarrier: (a) $\alpha = 0.5$, (b) $\alpha = 0$. In both figures the amplitude and phase of the interference stay the same.

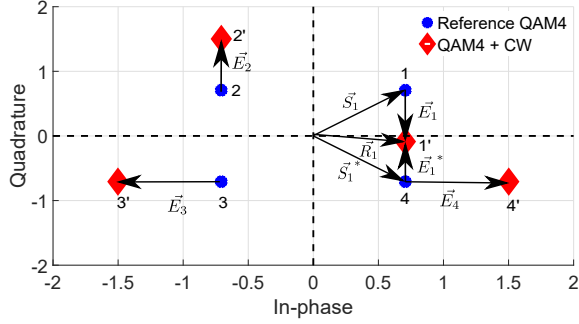


Fig. 3: CW EMD influence on QPSK modulated symbols

symbol flip (i.e. the estimated $S_m^* = S_m$ and $E_m^* = E_m$), as shown in three out of four quadrants in Fig. 3. Next, applying the DFT on (7) and implementing an ideal automatic gain control as shown in (8) result in the equations (10) and (11) for S_m and E_m , respectively.

$$\begin{aligned} S_m &= 2 \sum_{n=0}^{K-1} \left(\left(\frac{a_n}{2} + j \frac{b_n}{2} \right) e^{-j2\pi mn/K} \right) \\ &= \frac{1}{K} \sum_{n=0}^{K-1} \left(\sum_{k=0}^{K-1} (I_k + jQ_k) e^{j2\pi kn/K} e^{-j2\pi mn/K} \right) \\ &= I_m + jQ_m \end{aligned} \quad (10)$$

$$E_m = A_{CW} \sum_{n=0}^{K-1} \left(e^{-j(2\pi f_{diff}n/Bd + \theta_{CW})} e^{-j2\pi mn/K} \right). \quad (11)$$

Note that after the DFT, the signal is transformed into the frequency-domain, where $t = \frac{n}{Bd}$.

Taking into account (5), equation (11) becomes:

$$\begin{aligned} E_m &= A_{CW} \sum_{n=0}^{K-1} \left(e^{-j(2\pi((d+\alpha)H)n/Bd + \theta_{CW})} e^{-j2\pi mn/K} \right) \\ &= A_{CW} e^{-j\theta_{CW}} \sum_{n=0}^{K-1} \left(e^{-j2\pi n(d+\alpha+m)/K} \right). \end{aligned} \quad (12)$$

E_m can be retrieved by subtracting the received symbol values R_m from the originally transmitted symbols S_m .

Combining (9) and (12) gives:

$$\begin{aligned} E_m &= R_m - S_m \\ &= A_{CW} e^{-j\theta_{CW}} \sum_{n=0}^{K-1} \left(e^{-j2\pi n(d+\alpha+m)/K} \right). \end{aligned} \quad (13)$$

Note that (13) results in (14) if there is no spectral leakage ($\alpha = 0$):

$$E_m = \begin{cases} A_{CW} e^{-j\theta_{CW}} K & \text{if } m = -d \\ 0 & \text{if } m \neq -d \end{cases}. \quad (14)$$

The mathematical procedures described above can be represented by Fig. 4. The received QAM symbols R_m after demodulation can either be correct or erroneous. By remodulating the demodulated R_m , an estimation, S_m^* , of the original S_m is obtained. Which in its turn can lead to an estimation (E_m^*)

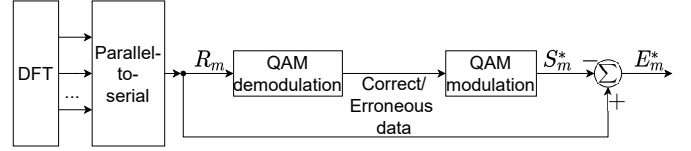


Fig. 4: The CW EMD extraction procedure

of the original E_m by subtracting R_m from the remodulated symbols S_m^* .

If the symbols were erroneously demodulated, then not all the S_m^* values will coincide with the originally transmitted symbol values S_k (see Fig. 1), and E_m^* will not be the actual E_m on certain subcarriers due to symbol flips.

An example of the CW EMD component large enough to cause symbol flips is shown in Fig. 5a and Fig. 5b for the real and imaginary parts, respectively. In both figures, the black line shows the error value E_m^* , the blue points show the received and remapped symbols S_m^* , while the red points show the originally transmitted symbols S_k . The black line, E_m^* clearly follows the spectral leakage pattern known from [20] except for the subcarriers 32 to 35, where a difference and, hence, a symbol flip of S_m^* with regards to S_k are also visible. The figures show that although some E_m^* values are no longer spectral leakage errors as defined in (13) for $m \in [32 : 35]$, all others still are.

C. Finding the CW EMD parameters

The previous subsection showed that when spectral leakage occurs ($\alpha \neq 0$), each subcarrier contains information about CW EMD represented as E_m^* values. In this subsection, let us assume that E_m^* fully equals E_m , i.e. the power of the CW EMD is too low to cause any symbol flips. The parameters of the CW EMD can then be found by exploiting a specific relation between the first and second half of subcarriers containing E_m . Let us show this mathematically, starting with the addition of E_m and $E_{m+\frac{K}{2}}$. Note that the integer operations on indices are ring-mapped back to the set, meaning that $m = K+1$ maps to 1 and $m = 0$ maps to K , i.e. modulo K calculus.

$$\begin{aligned} E_m + E_{m+\frac{K}{2}} &= \\ A_{CW} e^{-j\theta_{CW}} \sum_{n=0}^{K-1} \left(e^{-j2\pi n(d+\alpha+m)/K} (1 + e^{-j\pi n}) \right), \end{aligned} \quad (15)$$

with,

$$1 + e^{-j\pi n} = \begin{cases} 2 & \text{if } n \text{ is even} \\ 0 & \text{if } n \text{ is odd} \end{cases}.$$

By introducing $n = 2q$, the sum in (15) can be reduced (excluding all zeros) to a new sum (16):

$$\begin{aligned} E_m + E_{m+\frac{K}{2}} &= \\ 2A_{CW} e^{-j\theta_{CW}} \sum_{q=0}^{\frac{K}{2}-1} \left(e^{-j4\pi q(d+\alpha+m)/K} \right). \end{aligned} \quad (16)$$

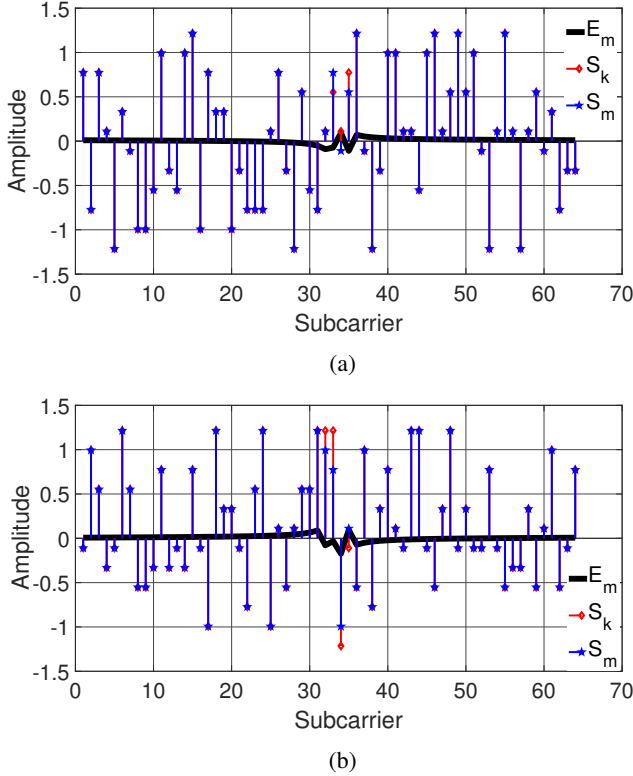


Fig. 5: QAM128 with 64 subcarriers: (a) — real part, (b) — imaginary part. E_m^* denotes CW EMD, S_m^* — received QAM symbols after "demodulation-modulation" process (see Fig. 4), S_k — transmitted QAM symbols (see Fig. 1).

Similarly to (15) and (16), let us now take the difference between E_m and $E_{m+\frac{K}{2}}$ and conduct the same operations:

$$E_m - E_{m+\frac{K}{2}} = A_{CW} e^{-j\theta_{CW}} \sum_{n=0}^{K-1} \left(e^{-j2\pi n(d+\alpha+m)/K} (1 - e^{-j\pi n}) \right), \quad (17)$$

with,

$$1 - e^{-j\pi n} = \begin{cases} 2 & \text{if } n \text{ is odd} \\ 0 & \text{if } n \text{ is even} \end{cases}.$$

By introducing $n = 2q + 1$, the sum in (17) can be reduced (excluding all zeros) in to a new sum (18):

$$\begin{aligned} E_m - E_{m+\frac{K}{2}} &= 2A_{CW} e^{-j\theta_{CW}} \sum_{q=0}^{\frac{K}{2}-1} \left(e^{-j2\pi(2q+1)(d+\alpha+m)/K} \right) = \\ &= 2A_{CW} e^{-j\theta_{CW}} e^{-j2\pi(d+\alpha+m)/K} \\ &\quad \times \sum_{q=0}^{\frac{K}{2}-1} \left(e^{-j4\pi q(d+\alpha+m)/K} \right). \end{aligned} \quad (18)$$

Looking at equations (18) and (16), one may notice that they depend on each other. This dependency allows to derive

the CW EMD frequency f_{diff} , what can be done by, first, combining expressions (18) and (16) that results in (19):

$$\begin{aligned} E_m - E_{m+\frac{K}{2}} &= (E_m + E_{m+\frac{K}{2}}) \left(e^{-j2\pi(d+\alpha+m)/K} \right) \\ &= (E_m + E_{m+\frac{K}{2}}) \left(e^{-j2\pi f_{\text{diff}}/Bd} e^{-j2\pi m/K} \right). \end{aligned} \quad (19)$$

The CW EMD frequency f_{diff} can then be derived from (19):

$$\begin{aligned} f_{\text{diff}} &= \frac{jBd}{2\pi} \ln \left(e^{-j2\pi f_{\text{diff}}/Bd} \right) \\ &= \frac{jBd}{2\pi} \ln \left(\frac{E_m - E_{m+\frac{K}{2}}}{E_m + E_{m+\frac{K}{2}}} e^{j2\pi m/K} \right). \end{aligned} \quad (20)$$

Once f_{diff} and E_m are known, the amplitude A_{CW} and phase θ_{CW} can also be calculated:

$$A_{CW} = \left| \frac{E_m + E_{m+\frac{K}{2}}}{2 \sum_{q=0}^{\frac{K}{2}-1} e^{-j4\pi q(f_{\text{diff}}/Bd+m/K)}} \right| \quad (21)$$

$$\theta_{CW} = j \ln \left(\frac{E_m + E_{m+\frac{K}{2}}}{2A_{CW} \sum_{q=0}^{\frac{K}{2}-1} e^{-j4\pi q(f_{\text{diff}}/Bd+m/K)}} \right). \quad (22)$$

As was shown in Figs. 3, 5a and 5b, if the CW EMD power is high enough, E_m^* is not always equal to E_m for one or more subcarriers (the subcarriers in Figs. 5a and 5b, where S_k and S_m^* do not coincide). However, one may use the E_m^* values from the subcarriers where no symbol flip occurred by the CW EMD (more details can be found in Section II-D). In this case, the estimation of f_{diff} , A_{CW} and θ_{CW} will be correct. It allows reconstructing CW EMD values, E_m , along subcarriers using (13). In Fig. 6 the real and imaginary parts of f_{diff} for the same example as in Figures 5a and 5b are shown. Taking into account equation (20), it can be seen that for subcarriers with imaginary part equal to zero ($m \in [2; 29]$) the real f_{diff} values can be used to make a correct estimation of CW EMD. For $m \in [1, 2, 3, 4]$, the imaginary part deviates from zero, thus these subcarriers cannot be used for CW EMD estimation, i.e. the correct f_{diff} can be found by looking for purely real f_{diff} . Eventually, the subtraction of E_m from the received symbols R_m will result in the originally transmitted S_k symbols.

D. The algorithm

In this subsection, all previous subsections are now combined to create the full algorithm, capable of removing the CW EMD influence on an OFDM frame. The full workflow to estimate the CW EMD and remove it from the OFDM frame is shown in Fig. 7. After retrieving E_m^* , f_{diff} is calculated using (20). Then the CW EMD amplitude and phase (A_{CW} and θ_{CW} , respectively) are determined according to (21) and (22). Knowing these parameters allows us to model the estimated CW EMD, subtract it from the disturbed OFDM symbol R_m and recover the original symbols.

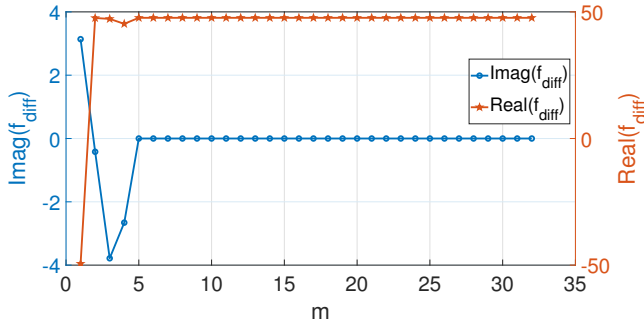


Fig. 6: Real and imaginary f_{diff} values for QAM128 with 64 subcarriers

The algorithm is designed in such a way that it starts working only when the maximum CW EMD (E_m^{max}) is greater than the quarter minimum Euclidean distance between adjacent points in the $I - Q$ constellation plane of the modulation scheme. In summary, the algorithm works as follows:

1. E_m^* values are found by demodulating-modulating received symbols according to (13).
2. f_{diff} is calculated for $m \in [0 : K/2]$, leading to a set of possible f_{diff} . If there are no symbol flips and no numerical errors, the full set would be real and exactly the same. However, this is not the case, so a number of steps were performed according to which specific f_{diff} values have to be taken:
 - A. The frequencies f_{diff} with the five imaginary parts $Im(f_{\text{diff}})$ close to zero are identified since a high deviation of the $Im(f_{\text{diff}})$ value from zero indicates an incorrect estimation of the f_{diff} .
 - B. Taking the median of the $Re(f_{\text{diff}})$ with the five least deviant from zero $Im(f_{\text{diff}})$ values results in the best performance.
3. The f_{diff} found in the previous step is used to calculate the CW EMD phase and the amplitude using (21) and (22).
4. The found CW EMD estimation is subtracted from the OFDM frame R_m after DFT.
5. The improved data symbols are demodulated.

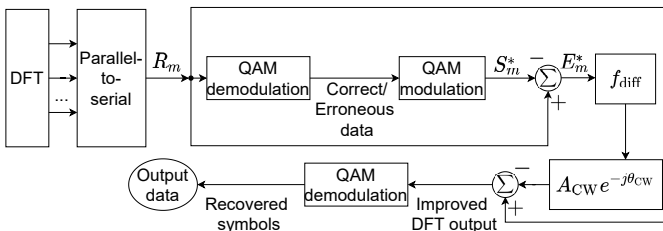


Fig. 7: CW EMD cancellation block diagram

TABLE I: Simulation parameters for OFDM symbols

Parameter	Value
Modulation scheme	QAM(M), M= [16; 32; 64; 128; 256; 512; 1024; 2048]
Number of subcarriers, K , divided by subcarrier width	[60; 120; 240; 510; 1020; 2040]
Number of bits, Y	$\log_2(M) \cdot K$
Baud rate, Bd	100
Coding technique	Hamming code(15,11)+interleaving
Subcarrier width, H	Bd/K

III. EVALUATION OF THE ALGORITHM

A. Simulation assumptions and main parameters

Before presenting simulation parameters and results, it is necessary to state the main assumptions which were made in this work:

- 1) perfect time and frequency synchronizations are present in the OFDM system.
- 2) perfect multipath fading compensation results in no need for the cyclic prefix and pilot signals.

The simulation of OFDM symbols and the interference was performed in MATLAB [21] at baseband frequencies. The OFDM symbols are constructed according to the simulation parameters shown in Table I. The interference is added to the OFDM symbol according to the parameters shown in Table II. For every possible EMD phase and every SIR, a new OFDM symbol is created with random input data. All results, shown in the following subsections, are then averaged over all EMD phases per SIR. This is repeated for different cases of modulation schemes, a number of subcarriers, and implementations (with and without the algorithm).

Note that when the CW EMD frequency is exactly on a subcarrier frequency ($\alpha = 0$), no spectral leakage occurs and the algorithm cannot find the CW EMD. It can, however, introduce an error (bit flips) on the data of that subcarrier. The CW EMD can be treated as a burst error, against which a simple row-column interleaving is effective [22]. With the help of interleaving, one may remove the bit flips spread among subcarriers using an error-correcting technique capable of correcting at least one bit flip. In this paper, the original bitstream is coded using the Hamming(15,11) code. Coding, along with interleaving, provides the needed result (elimination of CW EMD errors when $\alpha = 0$) with very limited overhead ($11/15 \approx 0.73$) and low computational cost.

B. Simulation results

With regards to the simulation parameters, the averaged (over 360 phases θ_{CW}) bit error rate (BER) was obtained through simulations for four different cases:

- 1) without the algorithm and coding technique;

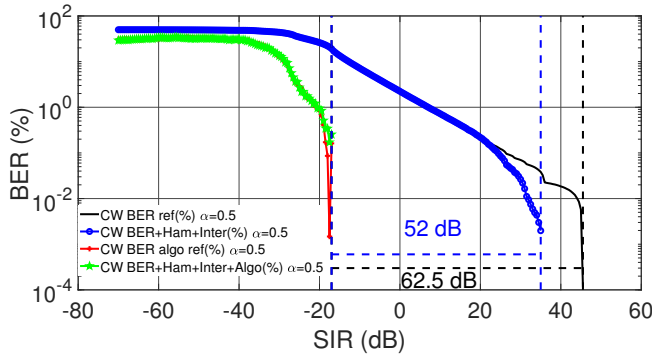


Fig. 8: CW EMD removal with the Hamming coding & interleaving for the OFDM packet with QAM64 modulation when $\alpha = 0.5$. $f_{diff} = 49.927$ Hz

- 2) only with the Hamming coding & interleaving [23];
- 3) only with the algorithm;
- 4) the algorithm along with the Hamming coding & interleaving.

Simulation results for QAM64 with 2040 subcarriers when $\alpha = [0; 0.25; 0.5]$ are presented on Figs. 8, 9 and 10.

In Fig. 8, the BER curves for $\alpha = 0.5$ are shown. The black curve shows the BER when neither the algorithm nor the error-correcting code is implemented. Note that the black curve has a sharp increase starting at approximately 45.5 dB SIR level. It is the point where CW EMD is just powerful enough to make one symbol error.

The blue BER curve shows the case where only the error correction technique and interleaving were implemented. It already shows a large benefit, mainly because CW EMD disturbs symbols whose subcarriers lie close to the f_{diff} frequency. When using the interleaving, the bit errors are spread over the complete OFDM frame and can to a large extent, be corrected by the Hamming coding. It shows a coding gain (the difference between the SIR levels between the message without the

TABLE II: Simulation parameters for CW EMD

Parameter	Value
CW EMD phase ^a (θ_{CW}), degree	[0:359]
Distance to the closest to CW EMD subcarrier ^b , α	[0; 0.25; 0.5]
SIR ^c span, dB	[-70:50]
SIR step, dB	0.1 dB
Noise amplitude ^d , A_{CW}	$A_{CW} = \frac{S_{RMS}}{10^{SIR/20}}$

^a Per each phase θ_{CW} , a new sequence of bits Y was generated;

^b f_{CW} and f_c are aligned in such a way that f_{diff} can take values between -50 Hz and 50 Hz;

^c $SIR = 20 \log_{10}(\frac{A_s}{A_{CW}})$, where A_s and A_{CW} denote the amplitude of the signal and interference, respectively;

^d S_{rms} is the root-mean-squared value of the signal in the time domain; SIR is the current SIR value.

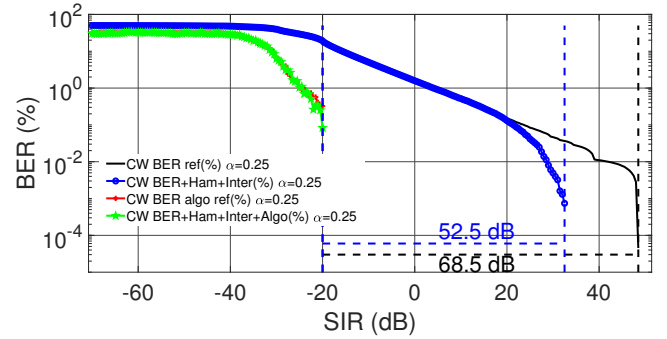


Fig. 9: CW EMD removal with the Hamming coding & interleaving for the OFDM packet with QAM64 modulation when $\alpha = 0.25$. $f_{diff} = 49.914$ Hz

error correction technique along with the interleaving and the message with them) of approximately 10.5 dB.

When the algorithm is used on its own (the red curved) or combined with the Hamming coding & interleaving (the green curve), the BER curve moves considerably to the left. The algorithm gain (the difference between the SIR levels between the message without the error correction technique along with the interleaving and the message with them and with the algorithm) in this case is 62.5 dB or 52 dB from the blue curve only implementing the error-correcting technique (first points of the red and green curves coincide).

Fig. 9 shows the BER curves when the CW EMD happens at a quarter of the subcarrier spacing from the nearest subcarrier ($\alpha = 0.25$). The results presented in Fig. 9 follow the same trend as in Fig. 8 with the following differences:

- 1) the gain of the Hamming coding & interleaving along with the CW EMD removal algorithm towards the Hamming coding & interleaving is 52.5 dB and towards the reference case (the black curve) is 68.5 dB;
- 2) the black, red, and green curves start at 48.5 dB and -20 dB (for the red and green curves), respectively.

Although the algorithm seems to work perfectly, it cannot detect and, therefore, remove the error when the CW EMD frequency is exactly equal to the subcarrier frequency ($\alpha = 0$).

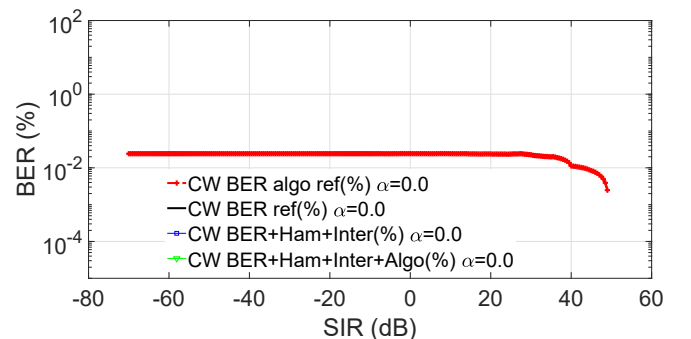


Fig. 10: CW EMD removal with the Hamming coding & interleaving for the OFDM packet with QAM64 modulation when $\alpha = 0$. $f_{diff} = 49.902$ Hz. The error correction technique results in nulled BER (blue and green curves).

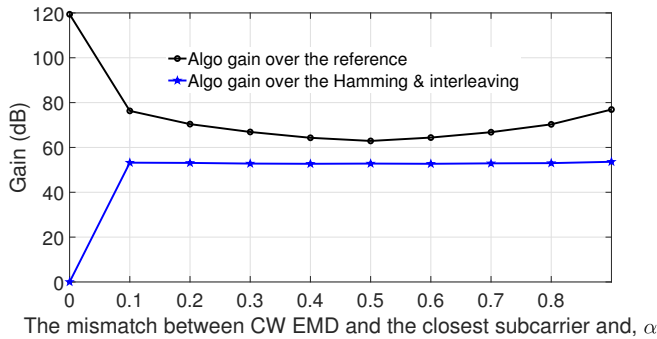


Fig. 11: CW EMD removal algorithm gain against α for QAM64 with 2040 subcarriers

However, as was mentioned in Section III-A, the combination of interleaving over all subcarriers and Hamming(15,11) code solves this issue. This can be noticed in Fig. 10, where the red curve (only the algorithm is applied) and the black curve (nothing is implemented, reference) are exactly the same. The other two cases, when the Hamming coding & interleaving were used (green and blue curves), result in BER = 0 throughout the whole SIR range and, hence, cannot be seen on the graph.

The algorithm's performance for different spectral leakage cases for QAM64 with 2040 subcarriers can be seen in Fig. 11. The black line corresponds to the algorithm gain calculated with regards to the minimal BER value for the reference case shown as the black line in Figs. 8—10. In the same fashion, the blue line is connected with the blue line in Figs. 8—10. The following comparison of Fig. 11 with Figs. 8—10 shows that the obtained gains depicted in Figs. 8—9 are particular cases of Fig. 11. For $\alpha = 0$ the blue line of Fig. 11 reaches zero because the implementation of the Hamming coding & interleaving results in no errors. For the black line, the gain reaches the maximum value because the algorithm + the Hamming coding & interleaving can deal with the error (BER=0). Without the algorithm and the Hamming coding & interleaving, the reference case has a constant BER value.

To show that the algorithm is effective for many different modulation orders M , as well as for a different number of subcarriers K , the simulation was performed for the modulation

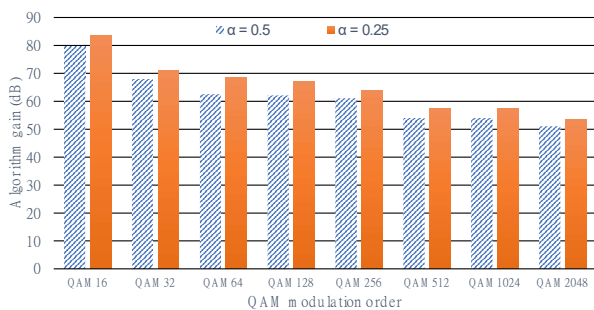


Fig. 12: CW EMD removal algorithm gain against QAM modulation order

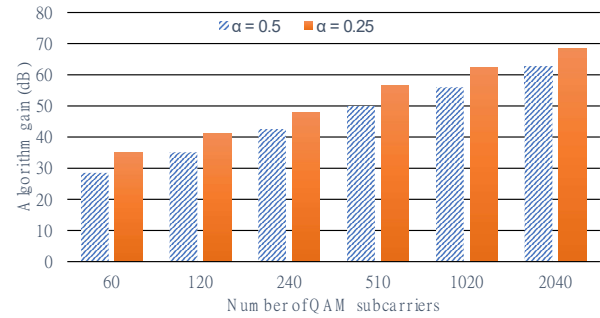


Fig. 13: CW EMD removal algorithm gain against a number of QAM subcarriers

order between QAM16 and QAM2048 with a fixed number of subcarriers of 2040 and a number of subcarriers between 60 and 2040 using QAM64. For each performed simulation, the algorithm gain is shown in Figs. 12 and 13.

As can be seen from Fig. 12, the CW EMD removal algorithm's performance deteriorates somewhat (from 79.5 dB for QAM16 to 51 dB for QAM2048) with the increase of the QAM modulation order. It happens due to the constant numerical noise. With the increase of the QAM modulation order M , the distance between symbols becomes smaller and the significance and influence of the calculation error become greater, thus reducing the performance of the algorithm.

In Fig. 13, an increase in the algorithm's gain occurs when the number of subcarriers increases. It can be explained as follows: CW EMD affects the same number of bits irrespective of the number of subcarriers. The increase of the latter increases the number of subcarriers K which can be correctly demodulated with the presence of CW EMD. In this way, the possibility to find the correct value of the disturbance frequency f_{diff} increases.

C. Performance evaluation under AWGN

In previous sections, the performance of the algorithm was discussed when perfect channel conditions were assumed. A simulation using 60 subcarriers with QAM64 modulation and for $\alpha = 0.5$ was done with AWGN having a signal-to-noise

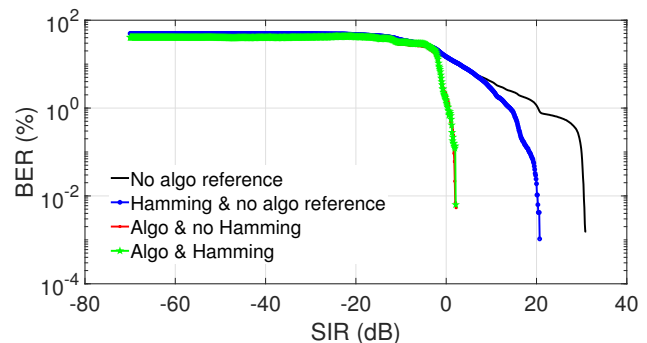


Fig. 14: CW EMD removal algorithm gain against $\alpha = 0.5$ for QAM64 with 60 subcarriers and AWGN at an SNR of 80 dB

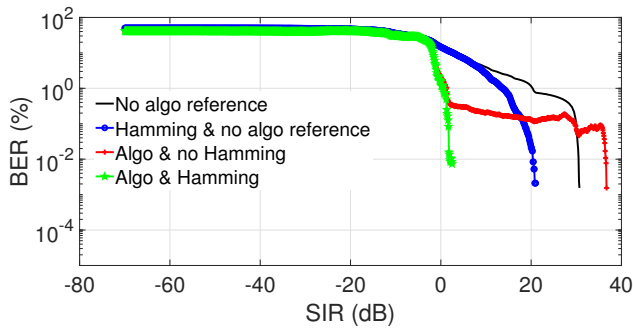


Fig. 15: CW EMD removal algorithm gain against $\alpha = 0.5$ for QAM64 with 60 subcarriers and AWGN at an SNR of 60 dB

(SNR) of 80 and 60 dB with regards to the original signal. The results for the SNR of 80 and 60 dB can be seen in Fig. 14 and Fig. 15, respectively. When the SNR is 80 dB, the performance of the algorithm, with or without the addition of Hamming error coding is as good as having no AWGN (shown in Fig. 13). When the SNR is 60 dB, the algorithm on its own appears to be heavily affected by the noise. Yet, with the addition of the Hamming coding & interleaving, the performance is still equal to the simulation case without AWGN.

IV. CONCLUSION

In this paper, a mathematical model and its validation for the CW EMD removal algorithm are described. The algorithm is compatible with QAM16—QAM2048 modulation schemes, exploits a spectral leakage phenomenon, and does not require any prior information about the disturbance. The only condition required for the algorithm is that CW EMD should not change within one OFDM packet. The algorithm is proposed as a measure of improvement of OFDM communication which is currently prevalent in digital communication.

The presented results demonstrate that by using the proposed CW EMD removal algorithm, one may achieve an algorithm gain of more than 80 dB. Adding simple coding techniques such as the Hamming coding & interleaving improves the algorithm’s performance for the non-spectral leakage case.

The proposed algorithm proved its efficiency, so the concept can be used for further improvements. In reality, AWGN with low SNR levels along with multiple CW EMDS can impede proper communication. This is especially relevant for autonomous vehicles that will be in the near future and where safety is of paramount importance. That is why further work will be focused on improving the current algorithm to withstand lower SNR levels and multiple CW EMDS.

REFERENCES

- [1] “Surface vehicle recommended practice,” SAE International, Warrendale, USA, Standard, Jun. 2018.
- [2] G. Naik, B. Choudhury, and J.-M. Park, “Ieee 802.11bd amp; 5g nr v2x: Evolution of radio access technologies for v2x communications,” *IEEE Access*, vol. 7, pp. 70 169–70 184, 2019.
- [3] A. Goldsmith, *Wireless communications*. Cambridge University Press, 2006.

- [4] T. Claeys, A. Ovechkin, D. Vanoost, G. A. E. Vandenbosch, and D. Pissort, “The need for and how to evaluate continuous wave immunity of wireless systems used in v2x applications,” in *2020 International Symposium on Electromagnetic Compatibility - EMC EUROPE*, Sep. 2020, pp. 1–6.
- [5] “WiFi/Bluetooth Jammers,” jammerfromchina.com. http://www.jammerfromchina.com/categories/WiFi%7B47%7DBluetooth_Jammers/, (accessed: October 13, 2021).
- [6] “Cell Phone Jammer,” jammer4uk.com. <https://www.jammer4uk.com/product-category/cell-phone-jammer>, (accessed: October 13, 2021).
- [7] K. Pelechrisinis, M. Iliofotou, and S. V. Krishnamurthy, “Denial of service attacks in wireless networks: The case of jammers,” *IEEE Communications Surveys Tutorials*, vol. 13, no. 2, pp. 245–257, Second 2011.
- [8] P. Ankarson, J. Carlsson, B. Bergqvist, S. Larsson, and M. Bertilsson, “Impact of different interference types on an lte communication link using conducted measurements,” in *2015 IEEE International Symposium on Electromagnetic Compatibility (EMC)*, Aug 2015, pp. 177–182.
- [9] K. M. Fors, K. C. Wiklundh, and P. F. Stenumgaard, “On the mismatch of emission requirements for cw interference against ofdm systems,” *IEEE Transactions on Electromagnetic Compatibility*, vol. 60, no. 5, pp. 1555–1561, Oct 2018.
- [10] M. Marey and H. Steendam, “Cancellation of digital narrowband interference formulti-carrier systems,” *Lecture Notes in Electrical Engineering*, vol. 1 LNEE, pp. 127–136, 2007.
- [11] K. Kang, J. Park, S. Hyoung, and J. Y. Oh, “Method and apparatus to cancel additive sinusoidal disturbances in OFDM receivers,” 2014.
- [12] T. Pande, I. H. Kim, and A. Batra, “A method for narrowband interference mitigation in ofdm by minimizing spectral leakage,” in *2015 IEEE International Symposium on Power Line Communications and Its Applications (ISPLC)*, March 2015, pp. 19–23.
- [13] D. Darsena, “Successive narrowband interference cancellation for ofdm systems,” *IEEE Communications Letters*, vol. 11, no. 1, pp. 73–75, Jan 2007.
- [14] D. Darsena and F. Verde, “Successive nbi cancellation using soft decisions for ofdm systems,” *IEEE Signal Processing Letters*, vol. 15, pp. 873–876, 2008.
- [15] A. Coulson, “Bit error rate performance of ofdm in narrowband interference with excision filtering,” *IEEE Transactions on Wireless Communications*, vol. 5, no. 9, pp. 2484–2492, Sep. 2006.
- [16] K. Fors, E. Axell, S. Linder, and P. Stenumgaard, “On the impact of cw interference on 5g nr,” in *2019 International Symposium on Electromagnetic Compatibility - EMC EUROPE*, Sep. 2019, pp. 1049–1054.
- [17] R. Nilsson, F. Sjoberg, and J. LeBlanc, “A rank-reduced lmmse canceller for narrowband interference suppression in ofdm-based systems,” *IEEE Transactions on Communications*, vol. 51, no. 12, pp. 2126–2140, Dec 2003.
- [18] T. Claeys, D. Vanoost, J. Peuteman, G. A. E. Vandenbosch, and D. Pissort, “Removing the spectral leakage in time-domain based near-field scanning measurements,” *IEEE Transactions on Electromagnetic Compatibility*, vol. 57, no. 6, pp. 1329–1337, Dec 2015.
- [19] T. Claeys, D. Vanoost, J. Peuteman, G. A. E. Vandenbosch, and D. Pissort, “An iterative interpolated dft to remove spectral leakage in time-domain near-field scanning,” *IEEE Transactions on Electromagnetic Compatibility*, vol. 60, no. 1, pp. 202–210, Feb 2018.
- [20] T. Claeys, “Increasing the accuracy and speed of emi near-field scanning,” 2018. [Online]. Available: <https://lirias.kuleuven.be/retrieve/512909>
- [21] MATLAB, 9.8.0.1323502 (R2020a). Natick, Massachusetts: The MathWorks Inc., 2020.
- [22] Y. Shi, X. M. Zhang, Z.-C. Ni, and N. Ansari, “Interleaving for combating bursts of errors,” *IEEE Circuits and Systems Magazine*, vol. 4, no. 1, pp. 29–42, 2004.
- [23] J. Van Waes, J. Lannoo, J. Vankeirsbilck, A. Degraeve, J. Peuteman, D. Vanoost, D. Pissort, and J. Boydens, “Effectiveness of hamming single error correction codes under harsh electromagnetic disturbances,” in *2018 International Symposium on Electromagnetic Compatibility (EMC EUROPE)*, Aug 2018, pp. 271–276.



Aleksandr Ovechkin was born in Tula, Russian Federation in 1995. He received the B.S. and M.S. degrees in electrical engineering from the National Research University Moscow Power Engineering Institute, Moscow, Russian Federation in 2016 and 2018, respectively. At the same university Mr. Ovechkin also obtained the B.S. degree in economics in 2018. He is currently pursuing the Ph.D. degree in the Electrical Engineering Department at Katholieke Universiteit (KU) Leuven, Bruges Campus, Bruges, Belgium.

From 2017 to 2018 he was an Electrical Design Engineer with Bastion. From 2018 to 2019 he was a Structural Design Engineer with Joint-Stock Company Atomstroyexport. His main research interest lies in dependable wireless connections capable of working under fault conditions in harsh electromagnetic environments.

Mr. Ovechkin's awards and honors include the Russian Presidential scholarship, the victory in the technical championship "The power of future", the award in the WorldSkills High-Tech 2018, the award of the international conference in National Research University Moscow Power Engineering Institute, a finalist of the best students' graduate qualification works contest and the award of the Moscow Olympiad in theoretical foundations in electrical engineering in National Research University Moscow Power Engineering Institute.



Guy A. E. Vandebosch received the M.S. and Ph.D. degrees in Electrical Engineering from KU Leuven, Leuven, Belgium, in 1985 and 1991, respectively.

Since 1993, he has been a Lecturer, and since 2005, a Full Professor at the same university. His research interests are in the area of electromagnetic theory, computational electromagnetics, planar antennas and circuits, nano-electromagnetics, EM radiation, EMC, and bio-electromagnetics. His work has been published in ca. 380 papers in international journals and has led to ca. 415 papers at international conferences. Guy Vandebosch has been a member of the "Management Committees" of the consecutive European COST actions on antennas since 1993. Within the ACE Network of Excellence of the EU (2004-2007), he was a member of the Executive Board and coordinated the activity on the creation of a European antenna software platform. After ACE, from 2007 – 2018, he chaired the EuRAAP Working Group on Software. In the period 1999-2004, he was vice-chairman, in the period 2005-2009 secretary, and in the period 2010-2017 chairman of the IEEE Benelux Chapter on Antennas en Propagation. In the period 2002-2004 he was secretary of the IEEE Benelux Chapter on EMC. In the period 2012-2014, he was secretary of the Belgian National Committee for Radio-electricity (URSI), where he is also in charge of commission E. Guy Vandebosch is a fellow of the IEEE. From September to December 2014, he was a visiting professor at Tsinghua University, Beijing, China. From 2017 to 2020 he was a member of the IEEE Electromagnetics Award Committee.



Tim Claeys was born in 1990. He received the M.S. degree in industrial engineering sciences, option electronics, from the University College Katholieke Hogeschool Sint-Lieven Gent, Ghent, Belgium, in 2013, and the Ph.D. degree in electrical engineering from KU Leuven, Leuven, Belgium, in 2018.

Since 2018, he has been a Postdoctoral Researcher with the M-Group Research Group (Lab FMEC), KU Leuven, Bruges, Belgium. His current research interests include near-field scanning, the development of characterization methods for shielding materials

and gaskets, electromagnetic interference resilience of wireless protocols, and global reliability of electronic systems. He is an IEEE member and part of the IEEE EMC Society Benelux chapter.



Davy Pissoort (M09, SM13) was born in 1978. He received the M.S. and Ph.D. degrees in electrical engineering from Ghent University, Ghent, Belgium, in 2001 and 2005, respectively.

From October 2005 to October 2006, he was a Postdoctoral Researcher at Ghent University. From November 2006 to July 2009, he was a Research Engineer in the Eesof-EDA Department, Agilent Technologies, Belgium. Since 2009, he is a professor at KU Leuven, Bruges Campus, where is the one of the principal investigators of the Mechatronics Group. His current research interests include the development of fast and efficient electromagnetic modeling methods for EMC, SI, and PI, the development of characterization methods for shielding materials and gaskets, EMI Resiliene, dependability of autonomous systems as well as the analysis and testing of the mechanical and thermal reliability of electronic modules. Dr. Pissoort is a Senior Member of the IEEE EMC Society, IEEE EMC Society Board Member and member of the International Steering Committee of EMC Europe.



Dries Vanoost was born in 1988. He received the M.S. degree from KU Leuven Technology campus Ostend, Ostend, Belgium, in 2010, and the PhD degree from KU Leuven, Leuven, Belgium, in 2015, both in electrical engineering.

Since January 2016, he has been a Postdoctoral Researcher at the M-Group research group, KU Leuven Bruges Campus, which is a laboratory focusing on global dependability of mechatronic systems and electromagnetic compatibility. His research interests include dependability of interconnected mechatronic

systems, electromagnetic modelling, power electronics, and power quality. He is an IEEE member and part of the IEEE EMC Society Benelux chapter.